The globular cluster system of the Auriga simulations

Timo L. R. Halbesma[1]⋆, Robert J. J. Grand[1], Volker Springel[1], Facundo A. Gómez[2,3], Federico Marinacci[4,5], Rüdiger Pakmor[1], Wilma Trick[1], Philipp Busch[1], Simon D. M. White[1]

[1] *Max-Planck-Institut für Astrophysik, Karl-Schwarzschild-Str. 1, 85741 Garching, Germany*
[2] *Instituto de Investigación Multidisciplinar en Ciencia yTecnología, Universidad de La Serena, Raúl Bitrán 1305, La Serena, Chile*
[3] *Departamento de Física y Astronomía, Universidad de La Serena, Av. Juan Cisternas 1200 N, La Serena, Chile*
[4] *Department of Physics, Kavli Institute for Astrophysics and Space Research, MIT, Cambridge, MA 02139, USA*
[5] *Harvard-Smithsonian Center for Astrophysics, 60 Garden Street, Cambridge, MA 02138, USA*

ABSTRACT

We investigate whether the galaxy formation model used for the Auriga simulations can produce a realistic globular cluster population at redshift zero. We compare properties of the simulated star particles in the Auriga haloes with catalogues of observations of the Milky Way and Andromeda globular cluster populations available in the literature. We find that the Auriga simulations do produce sufficient mass at radii and metallicities that are typical for the MW GCS, although we observe a varying mass-excess for the different $R_{\rm GC}$-[Fe/H] bins. This implies different values for the combined product of the bound cluster formation efficiency and the globular cluster disruption rate. Furthermore we test whether any of the Auriga galaxies has a metallicity and radial distribution that is consistent with the MW (M31) GCS. For any one of the Auriga haloes we reject the null hypothesis that the observed and simulated metallicities of GCs (GC candidates) are drawn from the same distribution at ≥ 98.32 % confidence level, for the GCS of the Milky Way as well as that of the Andromeda galaxy. The same holds true for the distribution of galactocentric radius. Overall, the Auriga simulations produce old star particles with higher metallicities than the MW and M31 GCS and at larger radii. The formation efficiency would have to linearly decrease with increasing metallicity for the Auriga GC candidates to be consistent with the MW GCS.

Key words: methods: numerical – galaxies: formation – galaxies: star clusters: general.

1 INTRODUCTION

Globular clusters (GC)s are old, bright, ubiquitous, and various properties of GC systems show correlations with their host galaxies. GC systems are believed to retain information about the galactic (gas) conditions at times of formation, thus, could offer unique insight into the (chemodynamical) evolution of their parent galaxies, if the formation and evolution of GCs- and GC systems themselves is adequately understood. However, despite decades of research (the extensive literature on GCs is summarised in several books and review articles, e.g. Harris 1991; Harris 2001; West et al. 2004; Brodie & Strader 2006; Gratton et al. 2012; Kruijssen 2014; Forbes et al. 2018), consensus on an exhaustive picture of the formation of GCs is yet to be reached.

The literature offers a wealth of formation scenarios. Peebles & Dicke (1968) and Peebles (1984) argue that GCs form as the earliest bound structures in the Universe (i.e. prior to formation of the main galaxy), noting that the Jeans length and mass shortly after recombination is consistent with typical GC masses and sizes. Diemand et al. (2005) and Boley et al. (2009) argue that (the blue subpopulations of) GCs form in biased dark matter halos at high redshift. Other recent hypotheses of GC formation prior to collapse of the proto-galaxy include formation in colliding supershells (Recchi et al. 2017), in supersonically induced gaseous objects (Chiou et al. 2019), or in high-speed collisions of dark matter subhaloes (Madau et al. 2019). Boylan-Kolchin (2017) suggests that (the blue subpopulation of) GCs could form

⋆ E-mail: Halbesma@MPA-Garching.MPG.DE

in high density regions along the cosmic filament before or during collapse.

Other models also date GCs formation during formation of the proto-galaxy itself, for example as a result of thermal instabilities in hot gas-rich haloes (Fall & Rees 1985, also see the discussions in Kang et al. 1990). Alternative formation trigggers are also explored, such as (other causes of) shock compression, or cloud-cloud colissions (e.g. Gunn 1980; Murray & Lin 1992; Harris & Pudritz 1994; Vietri & Pesce 1995; Larson 1996; Cen 2001).

Yet another hypothesis is that star cluster formation is triggered by (major) gas-rich (spiral) galaxy mergers (Schweizer 1987; Ashman & Zepf 1992), which is naturally expected within the framework of hierarchical assembly. One testable prediction of this scenario is the formation of young clusters in interacting and merging galaxies, which has been observed and are found to show remarkable similarities with globulars in the Milky Way (e.g. Whitmore & Schweizer 1995; Holtzman et al. 1996; Zepf et al. 1999; Whitmore et al. 1999). Moreover, modelling efforts of this framework yield GC (sub)populations consistent with various observables (e.g. Muratov & Gnedin 2010; Choksi et al. 2018), and the recent numerical simulation of an isolated dwarf-dwarf merger executed at very high resolution (baryonic mass $m_b \sim 4\mathrm{M}_\odot$; softening $\epsilon = 0.1$) produce star clusters that could be globular progenitors (Lahén et al. 2019).

As for the formation timeline, the scenarios (and flavours thereof) of Fall & Rees (1985) and Ashman & Zepf (1992) are intertwined because accretion and mergers continuously occurs trough out hierarchical build-up of galaxies. Various (other) hierarchical formation channels thus combine different aspects of the aforementioned paradigms, such as GC formation in (small) galactic disks before they are accreted onto an assembling galaxy (e.g. Côté et al. 2000, 2002; Beasley et al. 2002; Gnedin 2003). We refer to Gnedin et al. (2001) for a scoreboard of the aforementioned paradigms compared to observations of the Milky Way globular cluster system.

An idea that has recently been studied in detail is the hypothesis that the physical processes responsible for the formation of young massive clusters (YMCs, see Portegies Zwart et al. 2010, for a review), as observable in detail in the local Universe in great , also governs GC formation at high redshifts. In this framework, differences between both classes of objects are caused by nearly a Hubble time of (dynamical) evolution (e.g. Spitzer 1987). This picture is based on observed similarities between YMCs and GCs (e.g. Holtzman et al. 1992; Whitmore et al. 1999) and strengthened by observations of gravitationally lensed objects at high redshifts ($z = 2 - 6$). These sources have properties reminiscent of (local) YMCs and may be GC progenitors at times of formation (Vanzella et al. 2017; Johnson et al. 2017). The modelling work by Kruijssen et al. (2011, 2012); Kruijssen (2015) is now incorporated into cosmological zoom simulations and shows promising results (Pfeffer et al. 2018; Kruijssen et al. 2019).

Simulation resolutions have reached the mass range populated by GCs, and the gravitational force softening can be as low several parsec. A number of groups can thus incorporate formation of (globular) star clusters into their high-resolution hydrodynamical simulations. Ricotti et al. (2016) run parsec scale simulations of the high-redshift universe

prior to reionization (the simulations stop at $z = 9$), Li et al. (2017) implement a new subgrid model for star (cluster) formation and run simulations that reach $z = 3.3$, and the run of Renaud et al. (2017) reaches $z = 0.5$. Kim et al. (2018) find that mergers can push gas to high density that quickly forms clustered stars that end up tightly bound by the end of the simulation. A somewhat different approach couples semi-analytical models to DM-only simulations (Muratov & Gnedin 2010; Li & Gnedin 2014; Choksi et al. 2018; Choksi & Gnedin 2019b,a), as is done in the work by El-Badry et al. (2019).

In this work we use state of the art simulations that produce realistic spiral galaxies at redshift zero for which several global properties are consistent with the observations. The simulations yield realistic Milky Way analogues, and ~~such galaxies are known to~~ real galaxies host globular cluster systems. The question thus naturally arises whether the star formation histories of the simulations (also) ~~yield a population of star particles that is consistent with~~ give rise to a GC system similar to the Milky Way and/or Andromeda globular cluster systems. In particular, we ~~investigate~~ use the Auriga suite of cosmological zoom simulations (Grand et al. 2017, and described in Sec. 2) ~~because a study of its GC system could serve as an ultimate test of~~ to investigate whether the star formation model ~~.~~ implemented produces metallicity, radial, and metallicity-radial distributions that are consistent with the MW and/or M31 GC systems, and whether the model produces enough stellar mass with the right properties to allow for formation efficiencies lower than unity and the expected (dynamical) mass loss over the cluster lifetime (not modelled explicitly in this study).

The plan of the paper is as follows. We summarise the relevant characteristics of the Auriga simulations in section 2, followed by a summary of the observations of the Milky Way (MW) and Andromeda globular cluster system (GCS) in section 3 that we use to compare our simulations to in section 4. We discuss our findings in section 5 to come to our conclusions in section 6.

2   THE AURIGA SIMULATIONS

We use the Auriga simulations (Grand et al. 2017, hereafter G17), a suite of high-resolution cosmological zoom simulations of Milky Way-mass selected initial conditions. The simulations are performed with the AREPO (Springel 2010; Pakmor et al. 2016) code that solves the magnetohydrodynamical equations on a moving mesh. The galaxy formation model produces realistic spiral galaxies at redshift $z = 0$.

The interstellar medium is modelled using a sub-grid approach which implements the physical processes most relevant to galaxy formation and evolution. This model was tailored to the AREPO code and calibrated to reproduce key observables of galaxies, such as the history of the cosmic star formation rate density, the stellar mass to halo mass relation, and galaxy luminosity functions.

The sub-grid includes primordial and metal-line cooling with self-shielding corrections. Reionization is completed at redshift six by a time-varying spatially uniform UV background (Faucher-Giguère et al. 2009; Vogelsberger et al. 2013) The interstellar medium is described by an equation of state for a two-phase medium in pressure equilib-

rium (Springel & Hernquist 2003) with stochastic star formation in thermally unstable gas with a density threshold of $n = 0.13 \text{cm}^{-3}$, and consecutive stellar evolution is accounted for. Stars provide feedback by stellar winds (Marinacci et al. 2014; Grand et al. 2017), and further enrich the ISM with metals from SNIa, SNII, and AGB stars (Vogelsberger et al. 2013). The formation of black holes is modelled which results in feedback from active galactic nuclei (Springel et al. 2005; Marinacci et al. 2014; Grand et al. 2017). Finally, the simulations follow the evolution of a magnetic field of 10^{-14} (comoving) G seeded at $z = 127$ (Pakmor & Springel 2013; Pakmor et al. 2014). See G17 for further details of the numerical setup as well as the galaxy formation model.

The Auriga suite has a fiducial resolution level L4, accompanied by the lower (higher) level L5 (L3) that is available for selected initial condition runs. The baryonic mass resolution in order of increasing level is $m_b = [4\times10^5, 5\times10^4, 6\times10^3]$ $M_\odot$ with gravitational softening of collissionless particles $\epsilon = [738, 369, 184]$ pc. The mass resolution of the Auriga simulations is thus close to the characteristic peak mass of the lognormal GC mass distribution of 10^5 $M_\odot$ (Harris 1991), although the gravitational softening is two orders of magnitudes larger than typical GC radii. High-density gaseous regions are thus not expected to produce surviving stellar clumps with masses and radii consistent with GCs because such objects would numerically disperse, even in the highest-resolution runs. On the other hand, we can investigate (statistical) properties of age-selected GC candidates because each star particle represents a single stellar population with a total mass that could be consistent with one globular cluster. This means that their formation sites and that of a real-world GC may be consistent.

3 OBSERVATIONAL DATA

We describe the observations of the MW GCS in Sec. 3.1, and of the Andromeda (M31) GCS in Sec. 3.2

3.1 Milky Way

Harris (1996, 2010 edition; hereafter H96e10) provides a catalogue[1] of the Milky Way globular cluster system that contains properties of 157 GCs. The authors initially estimated the size of the MW GCS to be 180 ± 10, thus, their catalogue to be ~85% complete. However, an additional 59 GCs are claimed to have been discovered by various authors. The total number of GCs in the MW might add up to 216 with recent estimates now anticipating an additional thirty GCs yet to be discovered (e.g. Ryu & Lee 2018, and references therein). We still use data from the Harris catalogue, but caution that it may (only) be 53-72% complete. Specifically, the relevant data fields that we use from H96e10 are the metallicity [Fe/H], the Galactic distance components X, Y, and Z (in kpc)[2], and absolute magnitude in the V-band M_V. We use the latter to calculate mass-estimates by assuming

$M_{V,\odot} = 4.83$ and a mass to light ratio $M/L_V = 1.7$ $M/L_\odot$, the mean for MW clusters (McLaughlin & van der Marel 2005).

We supplement the catalogue with age-estimates from isochrone fits to stars near the main-sequence turnoff in 55 GCs (VandenBerg et al. 2013, hereafter V13). ~~The mean value of the age-estimates in this data set is 11.9 ± 0.1 Gyr and the dispersion is 0.8 Gyr. Furthermore, only one of the 55 GC age-estimates is below 10 Gyr.~~

3.2 Andromeda

The fifth revision of the revised bologna catalogue (RBC 5, last updated August, 2012) is the latest edition of three decades of systematically collecting integrated properties of the globular cluster system of the Andromeda galaxy (Galleti et al. 2004, and references therein). One contribution to RBC 5 is the work by Caldwell et al. (2011, hereafter C11), subsequently updated by Caldwell & Romanowsky (2016, hereafter CR16).

C11 and CR16 present a uniform set of spectroscopic observations calibrated on the Milky Way GCS of the inner 1.6° (~21) kpc that is believed to be 94% complete. GCs in the outer stellar halo, up to $R_{\text{proj}} \sim 150$ kpc, are observed in the Pan-Andromeda Archaeological Survey (PAndAS, Huxor et al. 2014, hereafter H14), but see also Veljanoski et al. (2014) and Mackey et al. (2019). H14 presents the discovery of 59 new GCs and publishes updates to RBC 5. The work of H14 is incorporated in the latest public release[3] of the C11 dataset, further revised by CR16. It seems that CR16 is the most recent aggregated dataset of M31's GCS that contains properties of interest for our study as it contains GCs in the inner region and in the outer halo. The relevant fields in the CR16 dataset that we use are the age, metallicity, and the mass-estimate[4].

3.3 Age-estimates

Figure 1 shows a histogram of the age-estimates of the 55 MW GCs in V13 and 88 GCs in M31 for which age-estimates are available in CR16. The mean age of the MW GCs in this data set is 11.9 ± 0.1 Gyr and the dispersion is 0.8 Gyr. Furthermore, only one of the 55 GC age-estimates is below 10 Gyr. The M31 GCS has a mean age of 11.0±0.2 Gyr with a dispersion of 2.2 Gyr, and 24 GCs have age-estimates below 10 Gyr with a minimum age of 4.8 Gyr. ~~We show a histogram of the age-estimates of the 55 MW GCs in V13 and 88 GCs in M31 for which age-estimates are available in CR16, see Figure 1.~~ The Milky Way appears to host a globular cluster system that is somewhat older than the Andromeda galaxy, although we caution that both data sets are incomplete and the age measurements have large uncertainties (of $1 - 2$ Gyr)

---

[1] See https://www.physics.mcmaster.ca/Fac_Harris/mwgc.dat
[2] In a Sun-centered coordinate system: X points toward Galactic center, Y in direction of Galactic rotation, and Z toward the North Galactic Pole. We calculate the galactocentric radius $R_{\text{GC}} = \sqrt{(X - R_\odot)^2 + Y^2 + Z^2}$, assuming the solar radius $R_\odot = 8$ kpc.

[3] Last revised 23 Sep 2015, see https://www.cfa.harvard.edu/oir/eg/m31clusters/M31_Hectospec.html
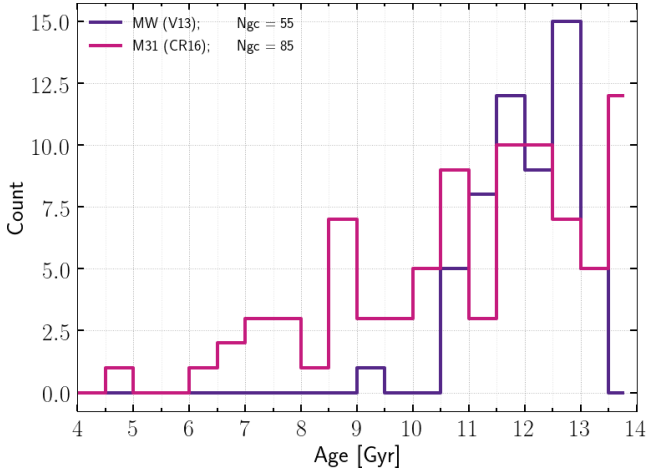[4] The authors assumed $M/L_V = 2$ independent of [Fe/H]

Figure 1. Age distribution of 55 GCs in the MW (data from VandenBerg et al. 2013) and 88 GCs in M31 (data from Caldwell & Romanowsky 2016).

3.4   Total GC mass in metallicity-radial space

We show the two-dimensional mass-weighted metallicity-radial distribution of the MW (M31) GCS in the top (bottom) panel of Figure 2. Both quantities are readily available in H96e10 (assuming $R_\odot$ = 8.0 kpc), but the galactocentric radius of GCs in M31 is not available in CR16. Therefore we follow Wang et al. (2019, Sec. 4.1) to calculate the projected radius $R_{\rm proj}$ from the observed positions, adopting M31's central position from the NASA Extragalactic Database[5] (α_0, δ_0) = $(0^{\rm h}42^{\rm m}44.35^{\rm s}, +41°16'08.63")$ and distance $D_{\rm M31}$ = 780 kpc (McConnachie et al. 2005; Conn et al. 2012) We calculate $R_{\rm GC}$ as 'average deprojected distance' $R_{\rm GC}$ = $R_{\rm proj} \times (4/\pi)$. The observations indicate that no GCs with high metallicities are to be expected at large radii (the three bins in the upper right corner, both for MW and M31), and relatively few GCs at large radii in general ($R_{\rm GC}$ > 30 kpc; right column: 11 GCs or 7.3% in the MW and 17 or 4.6% in M31). We compare these observations to the Auriga simulations later on in Sec. 4.3.

4   RESULTS

We define GC candidates in the Auriga simulations as all star particles older than 10 Gyr based on the age distribution of the MW GCS (Figure 1), and following the analysis of Renaud et al. (2017).

Trough out our analysis we compare the distributions of three subsets of star particles: *old stars* (age > 10 Gyr, or GC candidates), *old insitu* stars (defined as those bound to the most-massive halo/subhalo in the first snapshot that the particle was recorded), and *old accreted* star particles (those that have formed ex-situ and are bound to the most-massive halo/subhalo at z = 0). For comparison we also include the results for *all stars* (when no additional selection criterion is applied to the star particles). We consider the metallicity
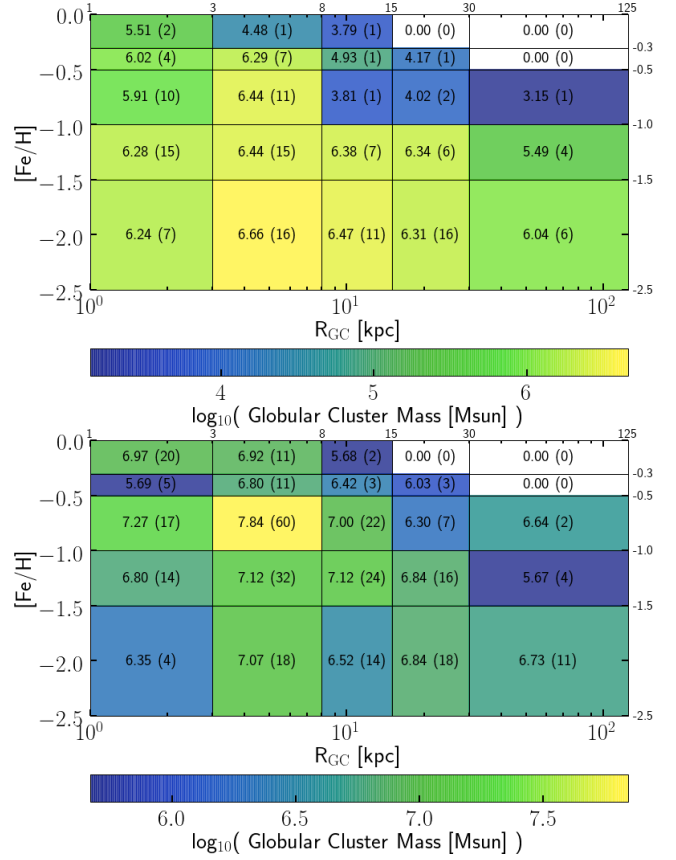
Figure 2. *Top*: Mass-weighted $R_{\rm GC}$-[Fe/H] distribution of 151 GCs in the MW (data from Harris 1996, 2010 ed.), which is 98.6 (92.2) % of the total mass (clusters) of the MW GCS in the Harris catalog. *Bottom*: Same for M31, showing 366 GCs and 88.4 (83.9) % of the total mass (clusters) in CR16 (data from Caldwell & Romanowsky 2016). Note that the range of the colourmap differs in both figures.

distribution in Sec. 4.1, the distribution of galactocentric radii in Sec. 4.2, and the combination of both in Sec. 4.3.

4.1   Metallicity distribution

We investigate whether the star formation model implemented in Auriga produces metallicity distributions consistent with the MW (and M31) GC systemGC systems, and whether the subgrid generates sufficient total mass at metallicities typical for the MW (and M31) GCSGCS's. To visually inspect the former we show the normalized metallicity distribution of three specific Auriga galaxies in Figure 3 in comparison to the MW and M31 [Fe/H] distributions.

Figure 3 shows the normalized metallicity distribution of We select Au4-10[6], Au4-21, and Au4-4 , showing the to show the distributions of three individual simulation runs that we consider representative for specific behaviour, and
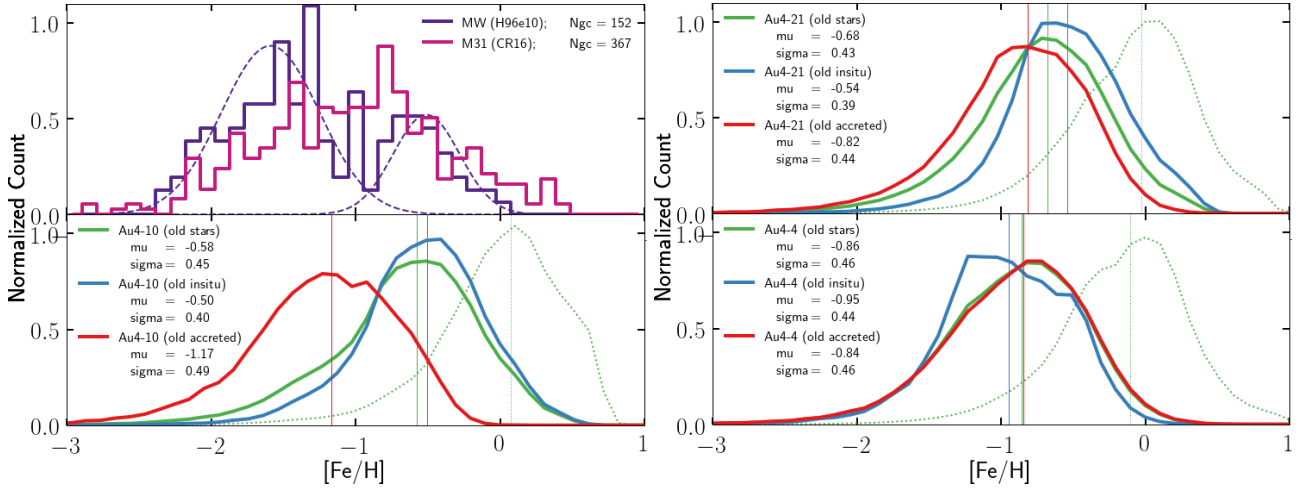
Figure 3. *Left:* Metallicity distribution of Au4-10 (bottom panel). We show the GG candidates in green. We split the GC candidates into two subpopulations, those that have formed insitu (blue), and those that have been accreted (red). The dotted green line shows all star particles. The solid purple (magenta) line in the top panel shows the GC system of the MW (M31). *Right:* Au4-4 (bottom), and Au4-21 (top).

to highlight that different runs could give rise to different distributions. We plot the age-selected GC candidates in green. ~~The accreted GC candidates are shown~~, those that are accreted in red, and the insitu subpopulation in blue. The top ~~panel~~ half of the left ~~panel~~ figure shows the MW (M31) GC system in purple (magenta)~~. We~~, where we overplot a double Gaussian for the MW GCS (the purple dashed lines) ~~,~~ by adopting literature values of the mean μ and standard deviation σ of the metal-rich and metal-poor ~~populations~~ subpopulations (Harris 2001, p. 38).

We find that the age cut, on average, lowers the mean metallicity from 0.0 to ~~−0.5~~−0.6. Furthermore, the old accreted stars generally have lower mean metallicities than the old insitu stars ~~. The difference between the mean metallicity of the old insitu and old accreted stars~~ with differences of roughly ~0.3 for the majority of the ~~simulations is ~0.3 (e.g. Au4-21), and~~ simulation runs. This behaviour can be seen in Au4-21, while a slightly larger difference of ~0.5 dex ~~for Au4-10~~is seen for Au4-10 (as plotted), Au4-16, Au4-17, Au4-18 and Au4-22. ~~This trend is only~~However, this trend is reversed for Au4-1 and Au4-4 ~~,~~for which the old insitu population has a lower mean metallicity instead. ~~For Au4-1~~We caution that Au4-1 is undergoing a major merger at redshift zero and note that we find $\mu = -1.51\,(-0.74)$ for the old insitu (accreted) ~~, but~~although the former consists of only 1019 particles (1.3% of all GC candidates, and with a total mass of 5e7 $M_\odot$)~~thus we believe our classification of insitu is flawed for this halo due to misclassification of the primary halo in the merger tree by subfind~~. For Au4-4, 10.8% of the GC candidates is classified as insitu (compared to insitu fractions of $40-80\%$ for other haloes). Overall we find that the simulations produce (sub)populations of GC candidates that are more metal-rich than the MW and M31 GC systems. Moreover, none of the simulations has a population of GC candidates with a bimodal metallicity distribution (the green curves).

We show the mean metallicity and standard deviation of all thirty Auriga L4 haloes in Figure 4 to show the behaviour for the full set of Auriga galaxies. The green
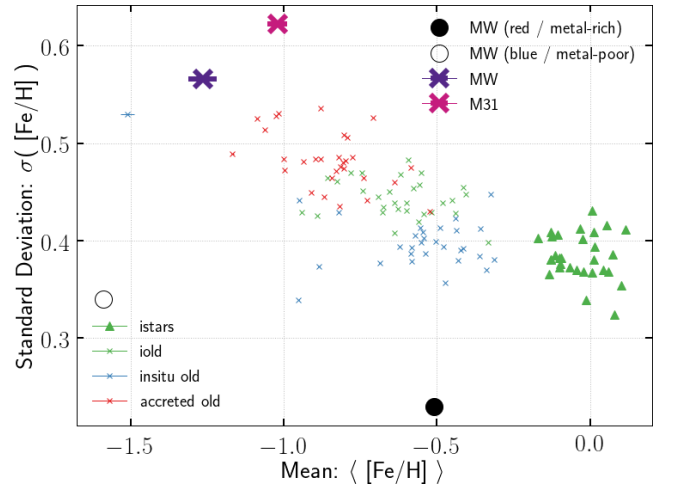

Figure 4. First vs second central moment of the Auriga L4 metallicity distributions. Each cross (for a given colour) represents one simulation. The green (blue) [red] crosses show the values calculated using the old (old insitu) [old accreted] star particles. Green triangles indicate that all stars were used. The purple (magenta) cross denotes our calculation using all MW (M31) observations (which would be appropriate for a unimodal distribution). The black solid (open) dots indicate the literature values of a bimodal Gaussian fit to the data (values from Ashman & Zepf 1998, p. 38), showing the metal-rich (metal-poor) component of the MW.

crosses are to be compared to the purple (magenta) cross, which shows the mean value of all MW (M31) GCs. ~~We~~In addition, we show the metal-rich (metal-poor) population of the MW GCS using a solid (open) dot. We caution that these literature values result from individual Gaussian fits to sub sets of the observational data cut at [Fe/H] = −1. We do not include corresponding data points calculated using such an artificial cut for the simulated star particles. Having said that, we do find it interesting that the mean metallicities of the old insitu populations appear roughly consistent with

that of the metal-rich population of the MW although the simulations show larger dispersions. The latter could simply be caused by the hard separation of the data into two groups, which means the range is smaller and the resulting dispersion could be lower. With regard to the M31 GCS, we are uncertain whether definitive consensus is reached concerning uni- bi- or trimodality in the [Fe/H] distribution, but CR16 argues that the data, after removal of younger objects due to improved age classification, hints at three populations separated at [Fe/H] > −0.4 and [Fe/H] < 1.5. None of the Auriga sub sets has a mean value that offers much hope that the simulated distribution is consistent with the lowest metallicity group in the M31 GCS. This is also true for the metal-poor population of the MW with a mean value of −1.6. The main take-away from this plot, again, is that all Auriga L4 galaxies have metallicity distributions with (much) larger mean values than what is observed for the MW and M31 GCS, and that we systematicly find lower mean metallicities for the accreted GC candidates than for those that have formed in situ.

Finally, we test the null hypothesis that MW (M31) and the GC candidates (all, insitu, and accreted) are drawn from the same underlying distribution by calculating the KS test statistic (i.e. six KS tests per simulation). We reject H_0 at the 100.00 % confidence level for virtually all subsets of all simulations, both for MW and M31, except when comparing the old accreted stars of Au4-10 to the MW GCS. In this case we still reject H_0 with, but with ≤ 98.68 % confidence. When comparing to the M31 GCS, the 'best' matches are the old accreted subpopulations of Au4-13, Au4-15, and Au4-17 (H_0 rejected with ≤ 99.82 % confidence, 99.95 %, and 98.32 %). Here we find that the cumulative distributions are more or less similar up to [Fe/H] −0.5, above which the simulations yield higher number counts which drives the KS test statistic over the critical values. This affirms our finding that the simulations produce GC candidates that are more metal-rich than the MW (M31) GCS. The main reasons that H_0 is rejected with such high confidence are under-production of old stars with [Fe/H] ≤ -1.5, and over-production of stars with [Fe/H]≥ -0.5.

In addition, we show the metal-rich (metal-poor) population of the MW GCS using a solid (open) dot. The mean metallicities of the old insitu populations appear roughly consistent with that of the metal-rich population of the MW, but the simulations show larger dispersions. We are uncertain whether definitive consensus is reached concerning uni- or bimodality in the Fe/Hdistribution of M31, but CR16 argues that the data, after removal of younger objects due to improved age classification, hints at three populations. However, we do not show these (unknown) points for the M31 GCS.

We now turn to the second goal, which is to see whether sufficient total mass in GC candidates produced by the Auriga simulations. To answer this question we plot a mass-weighted metallicity distribution in Figure 5. We show the median (coloured lines) for all thirty Auriga L4 haloes with the 1σ interval around it (shaded regions, which shows the scatter between runs that have different initial conditions, thus, have unique merger histories). We chose to aggregate the data to indicate a general trend general trends that we find when the GC candidates are split up according to birth location, rather than selecting typical ex-
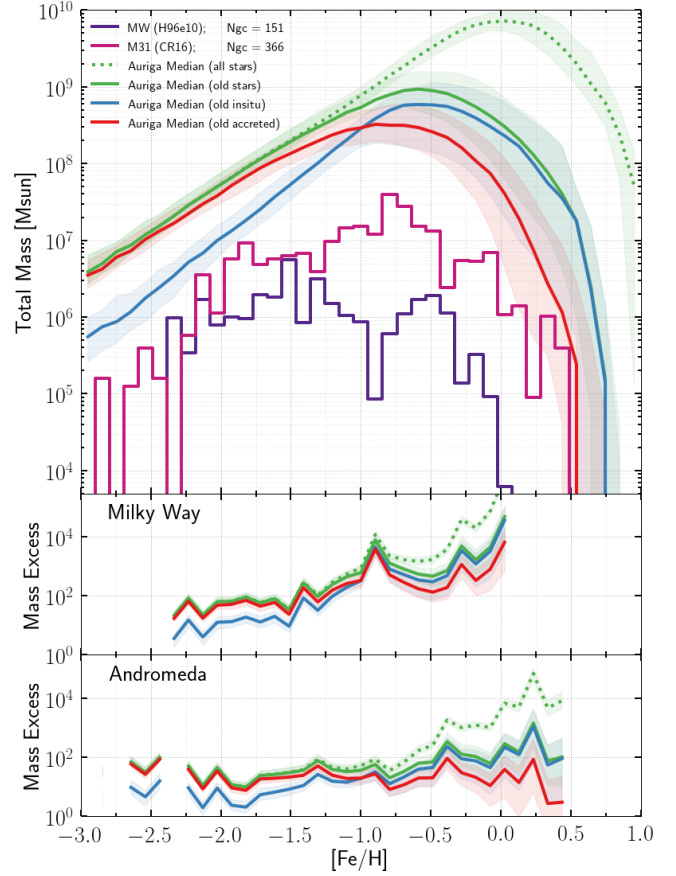

Figure 5. Mass-weighted metallicity distribution of star particles in the Auriga simulations. We show the median value of all Auriga haloes for all stars (green dotted) and globular cluster candidates (i.e. stars with age > 10 Gyr; green solid). The latter sub set is further split up between stars that formed in-situ (blue solid), and those that were accreted (red solid). Shaded regions indicate the 1σ interval. The MW (M31) GCS is shown in purple (magenta). The middle (bottom) panel shows the ratio of the simulated mass to the mass in the MW (M31) GCS.

amples of individual (simulated) galaxies. Figure 5 shows the mass-weighted metallicity distribution of all Auriga L4 galaxies. Once again we notice that the peak metallicity shifts down from 0 to −0.5 −0.6 for old stars (green solid) compared to all stars (green dotted), and we learn that the mass at the peak lowers by roughly one dex. The mass budget of the old stars is dominated by the old insitu population (blue solid) below [Fe/H] = −1, and by the old accreted stars (red solid) above this value. We show the MW (M31) GCS in purple (magenta) and we show the ratio of the simulated to the observed profiles in the middle (bottom) panel. This mass excess can be thought of the 'mass budget' that the Auriga GC candidates can 'afford to lose' due to a combination of smaller than unity bound cluster formation efficiencies combined with a Hubble time of dynamical evolution, while still producing a GC system with sufficient mass to be consistent with the MW (M31) GCS. The cluster formation efficiency would have to linearly decrease with decreasing metallicity for Auriga GC candidates to produce a population of GC candidates that is consistent with the MW. For
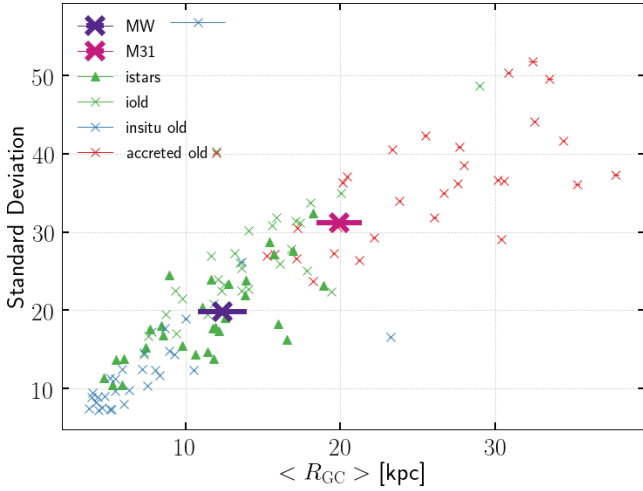
Figure 6. Mean and standard deviation of the radial distribution of star particles in each of the thirty Auriga L4 haloes compared to the MW (M31) GCS shown in purple (magenta).

the GC candidates in M31 we find a constant mass excess up to −0.9, above which the simulations produce a higher mass excess with increasing metallicity. If dynamical evolution is not expected to more efficiently disrupt GCs of higher metallicity, then we would find that the efficiency to form bound star clusters would have to decrease with increasing metallicity.

4.2 Radial distribution

Figure 6 shows the mean and standard deviation of the radial distribution of star particles in all Auriga L4 simulations. We notice that the old insitu populations are much more centrally distributed, whereas the old accreted component has a larger radial extent. Moreover, the dispersion increases with increasing mean value of the radial distribution as may be expected for a non-negative quantity.

Figure 7 shows the mass-weighted radial distribution of the Auriga L4 haloes. We notice a subtle peak around 10 kpc for all star particles that is not present for the GC candidates, indicating that the stellar disc is no longer present when applying the latter selection criterion. Furthermore, we find that the dominant contribution to the total mass in GC candidates changes from those formed insitu to the accreted population around 10 kpc. Again we show the mass excess of the simulations compared to the Milky Way and Andromeda GCS. We find a decreasing mass excess with increasing radius in the range 0.2 to ∼5 kpc, followed by an increase attributed to the accreted subpopulation. We further investigate a breakdown of the total mass in Auriga GC candidates into bins of both metallicity and radius in the following section.

4.3 Total mass in metallicity-radial space

We investigate whether the Auriga simulations still produce sufficient mass when the GC candidates are two-dimensionally binned in [Fe/H] and R_{GC}. First we sum the total simulated mass in each bin (for an individual Auriga
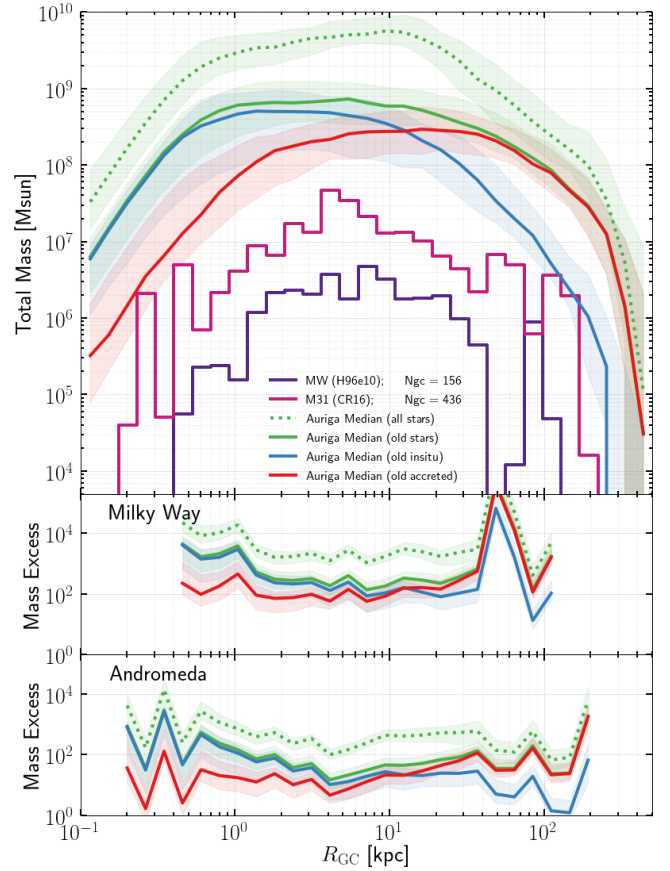
Figure 7. Mass-weighted radial distribution of star particles in the Auriga simulations. We show the median value of all Auriga haloes for all stars (green dotted) and globular cluster candidates (i.e. stars with age > 10 Gyr; green solid). The latter sub set is further split up between stars that formed in-situ (blue solid), and those that were accreted (red solid). Shaded regions indicate the 1σ interval. The MW (M31) GCS is shown in purple (magenta). The middle (bottom) panel shows the ratio of the simulated mass to the mass in the MW (M31) GCS.

simulation), then we calculate the median over all thirty Auriga L4 haloes (in each bin, see Figure 8 which can be compared to Figure 2). Finally, we divide these value by the total mass in the MW (M31) GCS to obtain the median mass excess produced by the star formation model implemented in the Auriga simulations. See the top (bottom) panel of Figure 9 for mass excess with respect to the MW (M31) GCS.

5 DISCUSSION

5.1 Metallicity distribution

Globular clusters are ∼0.5 dex more metal-poor than spheroid stars observed at the same radius for almost all galaxies (Harris 1991). Our selection function (age cut) does lower the mean metallicity by 0.5 dex, but we still find that the metallicity distributions of GC candidates in the Auriga simulations are more metal-rich than the MW (M31) GCS. Although the (old) star particles represent single stellar populations with a mass (resolution) consistent with that
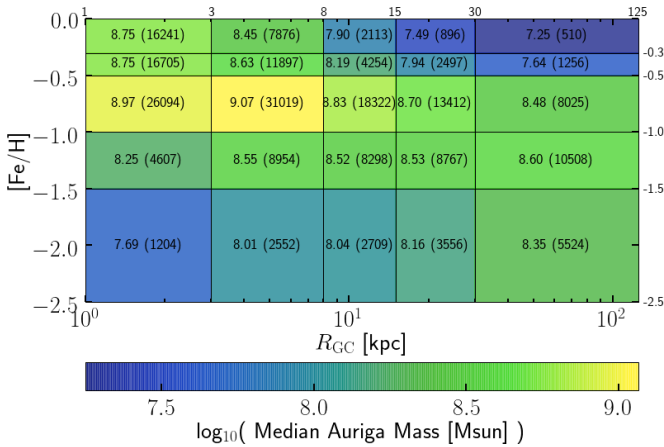
Figure 8. Mass-weighted [Fe/H]-R_{GC} distribution of all thirty Auriga L4 haloes. Here we consider only the GC candidates (age > 10 Gyr) stars in and color-code by the **median** (values also shown in each bin). The numbers in parenthesis show how many star particles fall within the bin. Note that the range of the colourmap again differs (for improved contrast within the plot).

of GCs, they are in fact statistical tracers of the stellar population of the galaxy as a whole. Therefore only a (small) fraction of the star particles may represent plausible formation sites of GCs, whereas the majority represents (halo) field stars - the disk component effectively falls outside our selection of star particles due to the age cut.

In general, the colour (metallicity) distribution of most GC systems is bimodal with typical separating value [Fe/H]~ −1 (Zinn 1985; Gebhardt & Kissler-Patig 1999; Larsen et al. 2001; Peng et al. 2006). Indeed, Ashman & Zepf (1998, p. 234) and Harris (2001, p. 38) find that the MW GCS has a bimodality [Fe/H] distribution: the latter fit a double Gaussian which peaks at [Fe/H] = −1.59 (metal-poor) and −0.51 (metal-rich) and dispersions of 0.34 and 0.23. Observations of GCs in M31, however, may best be split into three distinct metallicity groups, one found at small radii with [Fe/H] > −0.4, one intermediate [Fe/H] group, and a dominant (metal-poor) group with [Fe/H] < −1.5 (Caldwell & Romanowsky 2016). The numerical simulation of Renaud et al. (2017) does yield a bimodal metallicity distribution where the metal-poor population is dominated by accreted star particles and the metal-rich population by insitu stars.

We find that none of the Auriga simulations produces a bimodal metallicity distribution for age-selected GC candidates. Interestingly, the cross-over point above (below) which the mass-weighted metallicity distribution of GC candidates is dominated by those that have formed insitu (were accreted) does coincide with the separation between the metal-rich and metal-poor populations of GC systems at [Fe/H] = −1. Moreover, we do find that the mean metallicity shifts when we split the GC candidates up according to birth location (accreted or in-situ). In particular, the mean values of the old insitu GC candidates are roughly consistent with the metal-rich MW GCs. However, we also notice that a substantial number of simulations has similar mean values for all GC candidates, and the simulated insitu GC candidates have larger dispersions than the metal-rich GCs. Moreover, the offset between the mean of the metal-rich and
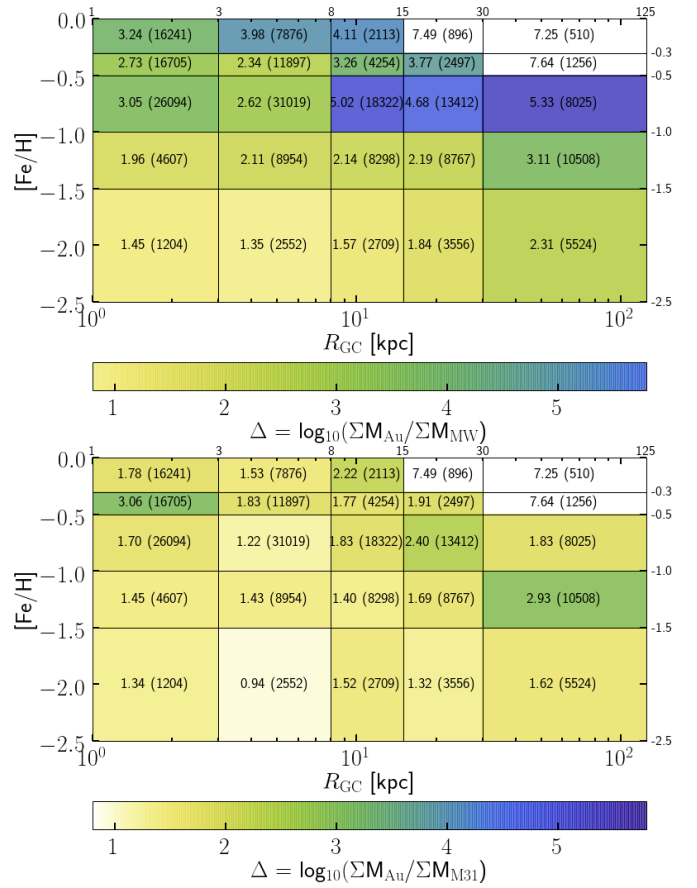

Figure 9. The top (bottom) panel shows the logarithm of the ratio of simulated mass to mass in the MW (M31) GCS, i.e. the logarithm of the mass excess. The color-coded values are also shown in each bin. Note that the three bins in the upper right corner are left blank because the observations have zero mass there, and that the numbers indicate how much (median) mass is produced by the simulations in those bins.

metal-poor populations in the MW is 1 dex, a factor $2 − 3$ larger than the offset that we find between the insitu and accreted populations. The Auriga simulations therefore do not support the view that the metal-poor GCs could have formed in satellites that have later been accreted whereas the metal-rich GC subpopulation has formed insitu. With this statement, however, we do caution that Kruijssen et al. (2019) suggests to reserve the 'ex situ' classification for accretion after $z = 2$, when the central galaxy has formed and accretion unambiguously contributes to the radially extended halo GC population. In fact, our classification appears flawed in Au4-1.

Finally, we note that Brodie & Strader (2006) compares the number of metal-poor GCs to the stellar halo mass and find[7] $T^n_{blue} \sim 100$, while the number of metal-rich GCs compared to the bulge mass yields $T^n_{red} \sim 5$, and therefore conclude that the formation efficiency of metal-poor GCs is twenty times higher than the metal-rich GCs with respect

---

[7] the quantity T is the number of GCs per 10^9 M$_\odot$ of galaxy stellar mass

to field stars. We find that gradual linear increase in formation efficiency of GCs with respect to field stars would be required with decreasing metallicity for the GC candidates in the Auriga simulations to yield sufficient total mass to be consistent with the Milky Way GCS.

5.2 Radial distribution

The M31 GCS has a factor 2-3 more GCs at large radii compared to the MW GCS, which may indicate that M31 has a richer merger history than the MW (Caldwell & Romanowsky 2016). In the Auriga simulations we find that the GC candidates at radii larger than ~20 kpc are indeed dominated by accreted star particles. However, we select star particles that are bound to the main halo and main subhalo, which means that we include particles up to the virial radius R_{200}. The Auriga simulations have no problem populating the stellar halo up to the virial radius, even with our additional age cut. On the other hand, the MW and M31 have fewer GCs at large radii. We expect tidal disruption to be less efficient at larger radii, thus, the formation efficiencies of the accreted GC candidates would have to be lower. Our classification as GC candidates could, for example, be improved by selecting a number of globular clusters based on the $M_{vir} - N_{GC}$ correlation found by Burkert & Forbes (2019), and taking a virial mass below which none of the star particles is treated as GC candidate.

5.3 Star particles are not globular clusters

Paraphrase the following

Reina-Campos et al. (2019) "Out of the cluster formation models considered, the 'no formation physics' model, in which both the CFE and the ICMF are fixed throughout cosmic time, is approximately equivalent to those studies that use 'particle-tagging' techniques to identify GCs in cosmological simulations (e.g. Tonini 2013, Renaud et al. 2017). We find that this cluster formation model continues to form GCs at a vigorous rate until the present time, which implies it overproduces the total GC mass in the Milky Way by a factor 5.5 relative to the mass formed in the fiducial model. Likewise, the continued formation of GCs in this model predicts the on-going formation of massive ($M > 10^5$ $M_\odot$) clusters with [Fe/H]< -0.5 should be observed in Milky Way-mass galaxies at $z = 0$. For these reasons, an environmentally independent cluster formation description is not compatible with observations."

6 SUMMARY AND CONCLUSIONS

We investigate GC candidates in the Auriga simulations and draw the following conclusions.

• The star formation model implemented in the Auriga simulations produces metallicity distributions that are more metal-rich the Milky Way and M31 globular cluster systems.
• We reject the null hypothesis H_0 for any one of the Auriga simulations that the GC candidates and the MW GCs are drawn from the same underlying distribution with ≥ 98.68 % confidence. This statement holds true when we select all old star particles (GC candidates), but also when

we select the old accreted or the old insitu star particles. In addition, this is also the case when we test against the M31 GCS instead of the MW GCS.
• GC candidates in the Auriga simulations may be found out to R_{200}, given that our selection function of star particles selects all stars bound to the main subhalo in the main halo. The stellar mass is dominated by accreted star particles at radii beyond 20 kpc. The GCs in the MW and M31, on the other hand, have a much smaller radial extend.
• The cluster formation efficiency would have to increase with decreasing metallicity for GC candidates in the Auriga simulations to be consistent with the Milky Way GC system, given that we expect dynamical evolution to more strongly affect GC candidates at smaller radii. This trent of overproduction of old star particles that are metal-rich and at large radii compared to observed GCs is less clear for the M31 GCS.
• The Auriga simulations are not consistent with the picture that all metal-rich GCs formed insitu and that all metal-poor GCs were accreted.

REFERENCES

Ashman K. M., Zepf S. E., 1992, ApJ, 384, 50
Ashman K. M., Zepf S. E., 1998, Globular Cluster Systems
Astropy Collaboration et al., 2013, A&A, 558, A33
Beasley M. A., Baugh C. M., Forbes D. A., Sharples R. M., Frenk C. S., 2002, MNRAS, 333, 383
Boley A. C., Lake G., Read J., Teyssier R., 2009, ApJ, 706, L192
Boylan-Kolchin M., 2017, MNRAS, 472, 3120
Brodie J. P., Strader J., 2006, ARA&A, 44, 193
Burkert A., Forbes D., 2019, arXiv e-prints,
Caldwell N., Romanowsky A. J., 2016, ApJ, 824, 42

Caldwell N., Schiavon R., Morrison H., Rose J. A., Harding P., 2011, AJ, 141, 61
Cen R., 2001, ApJ, 560, 592
Chiou Y. S., Naoz S., Burkhart B., Marinacci F., Vogelsberger M., 2019, arXiv e-prints,
Choksi N., Gnedin O. Y., 2019a, arXiv e-prints,
Choksi N., Gnedin O. Y., 2019b, MNRAS, 486, 331
Choksi N., Gnedin O. Y., Li H., 2018, MNRAS, 480, 2343
Conn A. R., et al., 2012, ApJ, 758, 11
Côté P., Marzke R. O., West M. J., Minniti D., 2000, ApJ, 533, 869
Côté P., West M. J., Marzke R. O., 2002, ApJ, 567, 853
Diemand J., Madau P., Moore B., 2005, MNRAS, 364, 367
El-Badry K., Quataert E., Weisz D. R., Choksi N., Boylan-Kolchin M., 2019, MNRAS, 482, 4528
Fall S. M., Rees M. J., 1985, ApJ, 298, 18
Faucher-Giguère C.-A., Lidz A., Zaldarriaga M., Hernquist L., 2009, ApJ, 703, 1416
Forbes D. A., et al., 2018, Proceedings of the Royal Society of London Series A, 474, 20170616
Galleti S., Federici L., Bellazzini M., Fusi Pecci F., Macrina S., 2004, A&A, 416, 917
Gebhardt K., Kissler-Patig M., 1999, AJ, 118, 1526
Gnedin O. Y., 2003, in Kissler-Patig M., ed., Extragalactic Globular Cluster Systems. p. 224 (arXiv:astro-ph/0210556), doi:10.1007/10857603_35
Gnedin O. Y., Lahav O., Rees M. J., 2001, arXiv Astrophysics e-prints,
Grand R. J. J., et al., 2017, MNRAS, 467, 179
Gratton R. G., Carretta E., Bragaglia A., 2012, A&ARv, 20, 50
Gunn J. E., 1980, in Hanes D., Madore B., eds, Globular Clusters. p. 301
Harris W. E., 1991, ARA&A, 29, 543
Harris W. E., 1996, AJ, 112, 1487
Harris W. E., 2001, Globular Cluster Systems. Springer Berlin Heidelberg, p. 223âĂŞ408, doi:10.1007/3-540-31634-5_2, https://doi.org/10.1007/3-540-31634-5_2
Harris W. E., Pudritz R. E., 1994, ApJ, 429, 177
Holtzman J. A., et al., 1992, AJ, 103, 691
Holtzman J. A., et al., 1996, AJ, 112, 416
Hunter J. D., 2007, Computing in Science and Engineering, 9, 90
Huxor A. P., et al., 2014, MNRAS, 442, 2165
Johnson T. L., et al., 2017, ApJ, 843, L21
Jones E., Oliphant T., Peterson P., et al., 2001, SciPy: Open source scientific tools for Python, http://www.scipy.org/
Kang H., Shapiro P. R., Fall S. M., Rees M. J., 1990, ApJ, 363, 488
Kim J.-h., et al., 2018, MNRAS, 474, 4232
Kruijssen J. M. D., 2014, Classical and Quantum Gravity, 31, 244006
Kruijssen J. M. D., 2015, MNRAS, 454, 1658
Kruijssen J. M. D., Pelupessy F. I., Lamers H. J. G. L. M., Portegies Zwart S. F., Icke V., 2011, MNRAS, 414, 1339
Kruijssen J. M. D., Pelupessy F. I., Lamers H. J. G. L. M., Portegies Zwart S. F., Bastian N., Icke V., 2012, MNRAS, 421, 1927
Kruijssen J. M. D., Pfeffer J. L., Crain R. A., Bastian N., 2019, MNRAS, 486, 3134
Lahén N., Naab T., Johansson P. H., Elmegreen B., Hu C.-Y., Walch S., 2019, arXiv e-prints,
Larsen S. S., Brodie J. P., Huchra J. P., Forbes D. A., Grillmair C. J., 2001, AJ, 121, 2974
Larson R. B., 1996, in Morrison H. L., Sarajedini A., eds, Astronomical Society of the Pacific Conference Series Vol. 92, Formation of the Galactic Halo...Inside and Out. p. 241
Li H., Gnedin O. Y., 2014, ApJ, 796, 10
Li H., Gnedin O. Y., Gnedin N. Y., Meng X., Semenov V. A., Kravtsov A. V., 2017, ApJ, 834, 69
Mackey A. D., et al., 2019, MNRAS, 484, 1756

Madau P., Lupi A., Diemand J., Burkert A., Lin D. N. C., 2019, arXiv e-prints,
Marinacci F., Pakmor R., Springel V., 2014, MNRAS, 437, 1750
McConnachie A. W., Irwin M. J., Ferguson A. M. N., Ibata R. A., Lewis G. F., Tanvir N., 2005, MNRAS, 356, 979
McLaughlin D. E., van der Marel R. P., 2005, ApJS, 161, 304
Muratov A. L., Gnedin O. Y., 2010, ApJ, 718, 1266
Murray S. D., Lin D. N. C., 1992, ApJ, 400, 265
Pakmor R., Springel V., 2013, MNRAS, 432, 176
Pakmor R., Marinacci F., Springel V., 2014, ApJ, 783, L20
Pakmor R., Springel V., Bauer A., Mocz P., Munoz D. J., Ohlmann S. T., Schaal K., Zhu C., 2016, MNRAS, 455, 1134
Peebles P. J. E., 1984, ApJ, 277, 470
Peebles P. J. E., Dicke R. H., 1968, ApJ, 154, 891
Peng E. W., et al., 2006, ApJ, 639, 95
Perez F., Granger B. E., 2007, Computing in Science and Engineering, 9, 21
Pfeffer J., Kruijssen J. M. D., Crain R. A., Bastian N., 2018, MNRAS, 475, 4309
Portegies Zwart S. F., McMillan S. L. W., Gieles M., 2010, ARA&A, 48, 431
Recchi S., Wünsch R., Palouš J., Dinnbier F., 2017, Ap&SS, 362, 183
Reina-Campos M., Kruijssen J. M. D., Pfeffer J. L., Bastian N., Crain R. A., 2019, MNRAS, 486, 5838
Renaud F., Agertz O., Gieles M., 2017, MNRAS, 465, 3622
Ricotti M., Parry O. H., Gnedin N. Y., 2016, ApJ, 831, 204
Ryu J., Lee M. G., 2018, ApJ, 863, L38
Schweizer F., 1987, in Faber S. M., ed., Nearly Normal Galaxies. From the Planck Time to the Present. pp 18–25
Spitzer L., 1987, Dynamical evolution of globular clusters
Springel V., 2010, MNRAS, 401, 791
Springel V., Hernquist L., 2003, MNRAS, 339, 289
Springel V., Di Matteo T., Hernquist L., 2005, MNRAS, 361, 776
VandenBerg D. A., Brogaard K., Leaman R., Casagrande L., 2013, ApJ, 775, 134
Vanzella E., et al., 2017, MNRAS, 467, 4304
Veljanoski J., et al., 2014, MNRAS, 442, 2929
Vietri M., Pesce E., 1995, ApJ, 442, 618
Vogelsberger M., Genel S., Sijacki D., Torrey P., Springel V., Hernquist L., 2013, MNRAS, 436, 3031
Wang S., Ma J., Liu J., 2019, arXiv e-prints
West M. J., Côté P., Marzke R. O., Jordán A., 2004, Nature, 427, 31
Whitmore B. C., Schweizer F., 1995, AJ, 109, 960
Whitmore B. C., Zhang Q., Leitherer C., Fall S. M., Schweizer F., Miller B. W., 1999, AJ, 118, 1551
Zepf S. E., Ashman K. M., English J., Freeman K. C., Sharples R. M., 1999, AJ, 118, 752
Zinn R., 1985, ApJ, 293, 424
van Rossum G., de Boer J., 1991, CWI Quarterly, 4, 283
van der Walt S., Colbert S. C., Varoquaux G., 2011, Computing in Science and Engineering, 13, 22

This paper has been typeset from a TEX/LATEX file prepared by the author.